

MiniBooNE Resistive Wall Current Monitor*

M. Backfish[†], Fermilab, Batavia, IL 60504, USA

May 14, 2013

Abstract

The purpose of this document is to better characterize the behavior of the resistive wall current monitor that is located in the MiniBooNE beamline just before the target. This resistive wall current monitor is used to obtain a longitudinal profile of the 8 GeV beam that is used to create neutrinos for the MiniBooNE experiment. New MicroBooNE experiments require a better understanding of asymmetries in longitudinal signals in order to fully characterize the expected neutrino flux within the detector.

1 Introduction

A charged particle beam traveling through a conductive metallic beam pipe produces electric and magnetic fields that in turn induce image charges and currents on the beam pipe wall. These “Wall Currents” are equal and opposite to the beam current [1]. A resistive wall current monitor, hence forward RWM, measures the image charge that flows along the beam pipe wall. To perform this measurement, a nonconductive ceramic gap is placed in the vacuum chamber and bridged by resistors. Ferrite cores are placed around the beam pipe before and after the gap to prevent currents from flowing through alternate paths thus forcing the wall currents to pass through the gap resistors. The beam output can be monitored across this resistive gap, thus the RWM output is just the gap impedance times the beam current [2].

The RWM in the MiniBooNE beamline is a Main Injector style as shown in figure 1. This detector has a bandwidth of 2 KHz to 4 GHz. The calibration port has a bandwidth of 2 KHz to 2 GHz. The gap impedance is 1 Ohm [2]. Data from the MI8 line RWM, upstream of the MiniBooNE RWM, can be seen in figure 2. The asymmetries in the individual bunch traces must be understood to know the expected neutrino flux in the experiments particle detector. This research is to better relate measured RWM signals with the actual longitudinal beam distribution.

*Operated by Fermi Research Alliance, LLC under Contract No. DE-AC02-07CH11359 with the United States Department of Energy.

[†]backfish@fnal.gov



Figure 1: RWM with outer cover removed to expose the gap, the ferrites and the electronics. This image was provided by Brian Fellenz and Jim Crisp [2]

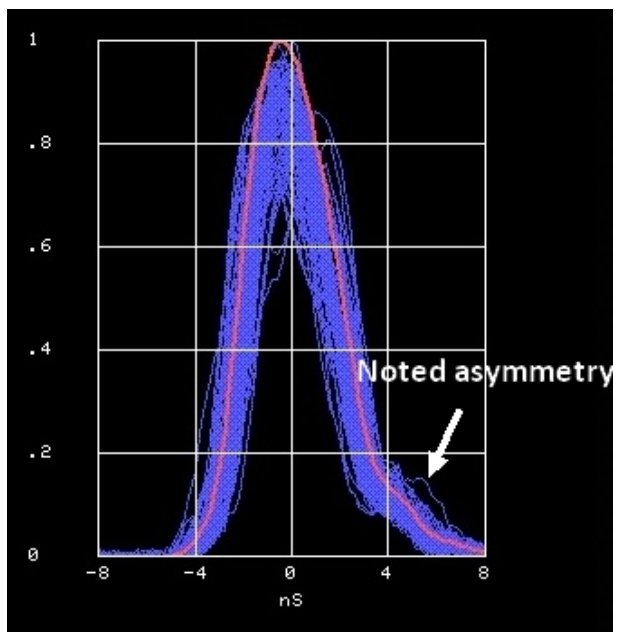


Figure 2: This data shows all 80 RWM traces and their average from the MI8 line which uses the same style of Resistive Wall Current Monitor.

2 Time Domain

The first step of this analysis is to insert a 5 V pulse that is 8 ns long into the calibration port on the RWM. The analysis is performed from the MI12 service building where the signal is sent through an RG58 cable with BNC connectors into a 1/2 inch heliax transmission line. This cable transports the pulse to the calibration port on the RWM. The calibration signal is then observed across the resistive gap ¹. The RWM signal from the detector travels through a 7/8 inch heliax cable to the MI12 service building where a short section of BNC terminated RG58 finishes the path to oscilloscope. The scope used for this part of the analysis is a 500 MHz digitizing oscilloscope used in equivalent time mode. In this mode the oscilloscope takes repeated data with slight timing offsets in order to obtain higher resolution [6]. A resolution of 4 ps was used for this analysis. The scope was also used in 1000 averages mode to help eliminate random noise. Figure 3 shows both the 8 ns input pulse and the RWM output together with a multiplier of -116 on the signal from the RWM.

The time domain data shown in figure 3 shows that a sharp rising signal in the range of a beam signal will have a leading edge that lags the actual signal and a falling edge that is slow to discharge. This type of roll-off can be a result of limited bandwidth and cable dispersion.

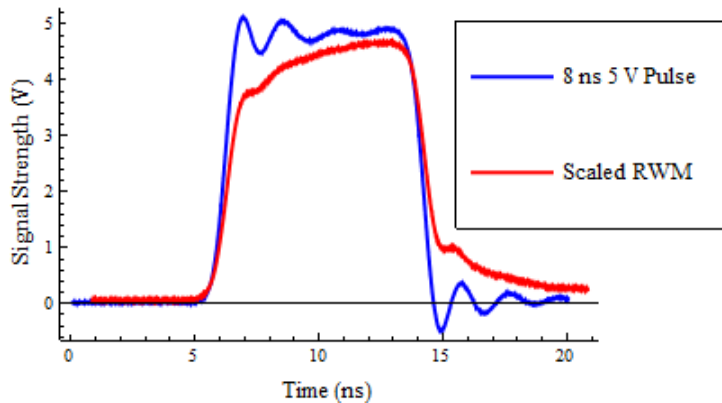


Figure 3: By observing a short pulse through the calibration port on the RWM across the resistive gap one can better determine the effects of the hardware limitations. The blue trace above is the 8 ns input pulse the red trace is the signal observed across the resistive gap multiplied times -116 to scale for the inversion and attenuation.

¹For a detailed description of the RWM circuit and calibration port see “Calibration of the Resistive Wall Monitor for the SBD and FBI Systems” by Jim Crisp and Brian Fellenz [3]

In the time domain an input signal, $x[n]$, convolved with a systems impulse response, $h[n]$, equals the output signal, $y[n]$, as shown in equation 1 where n is the sample number for a discrete signal.

$$x[n] * h[n] = y[n] \quad (1)$$

In the frequency domain an input spectrum, $X[f]$, multiplied by its frequency response, $H[f]$, is equal to its output spectrum, $Y[f]$. This is represented in equation 2 where f is the frequency.

$$X[f] \times H[f] = Y[f] \quad (2)$$

Since all of the data in this analysis consists of discrete signals, one can relate the time domain input and output signals to the frequency domain input and output spectrums through the discrete fourier transform as shown in figure 4. The Discrete Fourier Transform (or DFT) of the time domain input signal, $x[n]$, is equal to the input frequency spectrum, $X[f]$. The DFT of the impulse response, $h[n]$, is equal to the frequency response of the system, $H[f]$, and the DFT of the time domain output signal, $y[n]$, is equal to the output spectrum, $Y[f]$. There is a one to one correspondence between the impulse response and the frequency response as both contain complete information about the system [5].

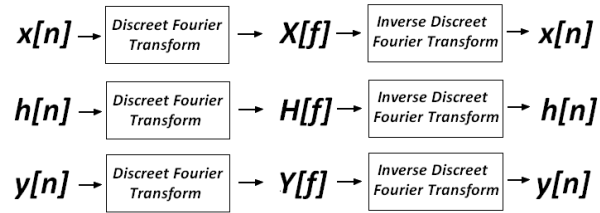


Figure 4: The time domain parameters of equation 1 are related to the frequency domain parameters of equation 2 through the discrete and inverse discrete fourier transforms.

Since the time domain output signal of a system is related to its input signal through the convolution of the input signal with its impulse response, the input and output time domain signals of Figure 3 can be used to calculate the impulse response of the RWM through the calibration port and cables. The impulse response, shown in figure 5, was found by deconvolving the measured input signal with the output signal.

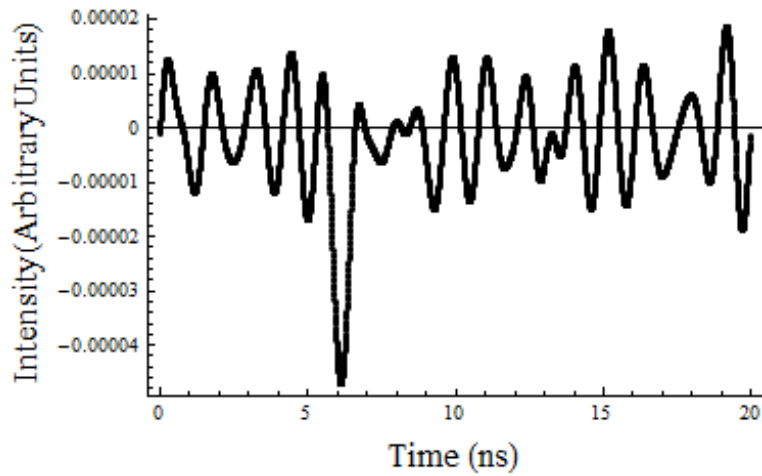


Figure 5: The measured impulse response of the MI12 RWM through the calibration port and cables

3 Application of the Impulse Response

The impulse response found can be convolved with known signals to determine the attenuation factor of the system and the shaping effects on a known signal. The gaussian function shown in equation 3 was divided into 4993 points between -0.05 and $+0.05$ in order to create a table of discrete values. This table was convolved with the experimentally found impulse response from section 2 above. Since the attenuation factor is only multiplied by the X axis for a time domain signal, the integral of that signal will also be scaled by that same factor. The attenuation factor is found by integrating, or in this discrete case summing the values from $n=1$ to $n=(\text{table length})$, for each table of values and finding the ratio between the two tables. In this case the output signal is $\frac{1}{116}$ of the input signal.

In figure 6 the output signal is multiplied by -116 in order to observe the signal on the same scale as the input signal. This shows that the measured impulse response of the RWM system causes an output signal to have a slower leading edge rise time and a sustained trailing edge.

$$V(t; a, \sigma) = a \times e^{\frac{-t^2}{2 \times \sigma^2}} \quad (3)$$

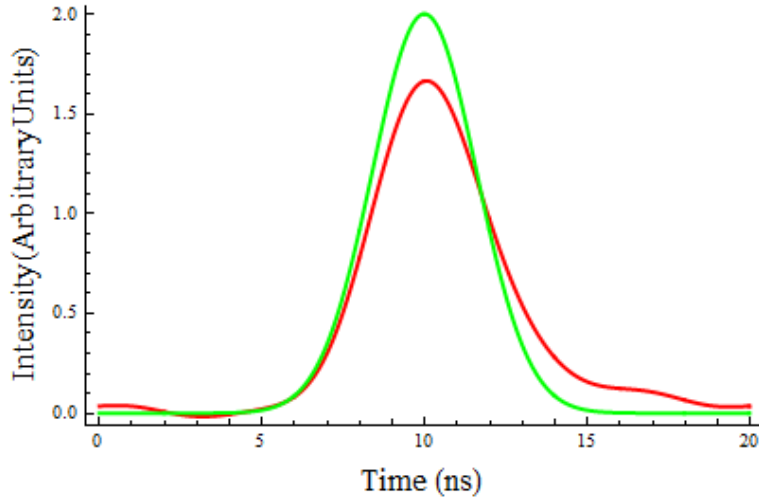


Figure 6: By convolving the impulse response found from the time domain measurements with a Gaussian function, the hardware effects on a Gaussian shaped beam can be better understood. The system response adds a rolloff to the leading edge and pedestal to the trailing edge.

4 Frequency Domain

To better analyze the frequency response of the system, a 2 MHz to 4 GHz network analyzer was used to perform an S21 measurement. The measurement was averaged 10 times with 1001 samples between 2 MHz and 4 GHz and is shown in figure 7. As discussed in section 2, the frequency response in the frequency domain is related to the impulse response in the time domain by the discrete fourier transform. By taking the inverse fourier transform of the frequency response, the impulse response is obtained as shown in figure 8. By convolving this impulse response with the original 8 ns pulse from the time domain measurements of section 2 we find that the impulse response measured through network analysis indeed shapes the pulse in a consistent manner with what is measured in section 2. This is displayed in figure 9. Figure 10 shows this impulse response convolved with a 4 ns FWHM Gaussian curve. This shows that the system adds a rolloff to the leading edge and a pedestal to the trailing edge. The asymmetry is consistent with that of the time domain measurements from section 2.

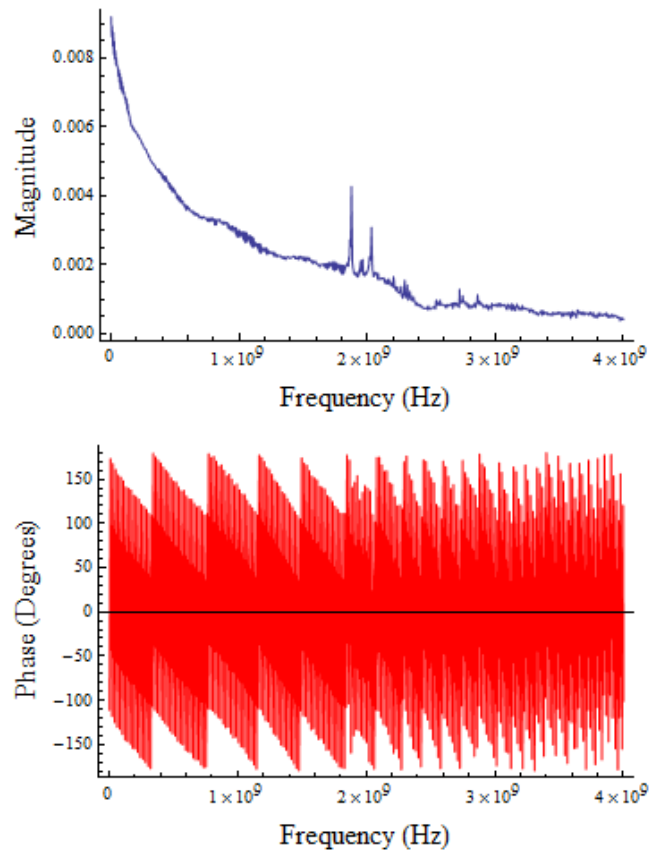


Figure 7: Frequency response through network analysis

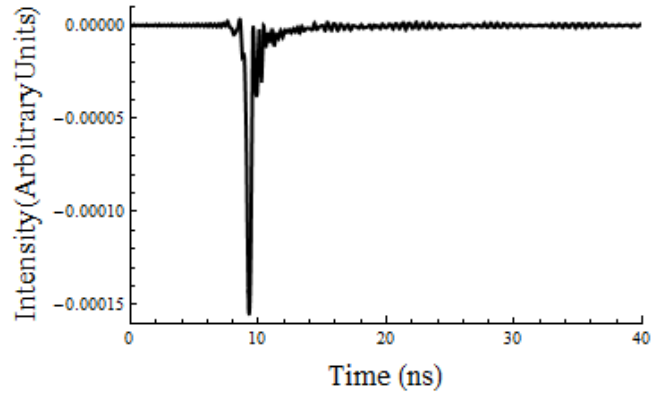


Figure 8: Impulse response found by taking the inverse discrete Fourier transform of the frequency response

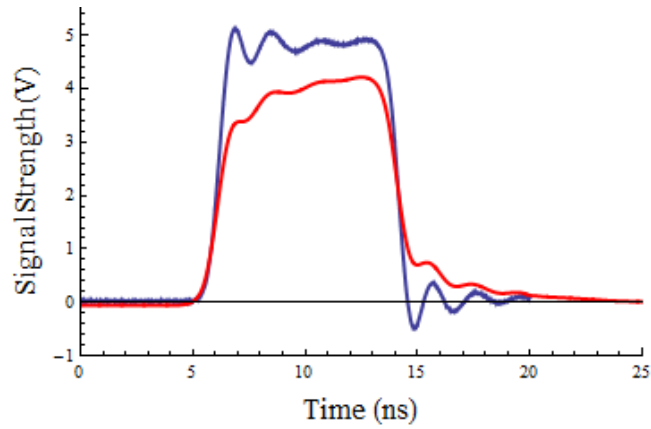


Figure 9: The blue trace is the original 8 ns input signal. The red signal is the input signal convolved with the impulse response found from the measured frequency response.

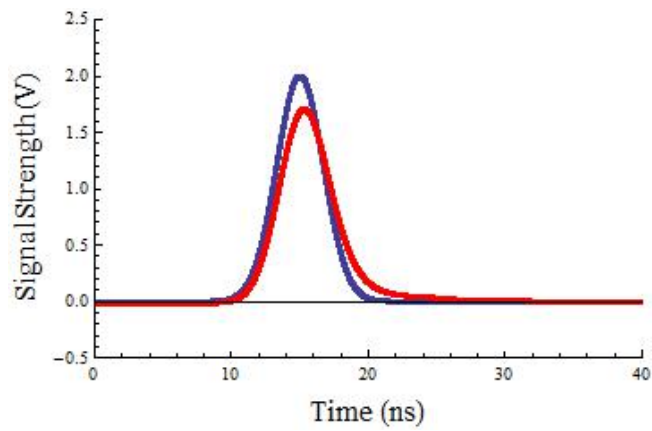


Figure 10: By convolving Gaussian functions with the impulse response calculated from the inverse fourier transform of the frequency response measurement one can see the effect on a signal similar to that of the beam. The system response adds a rolloff to the leading edge and pedestal to the trailing edge as seen earlier in figure 6.

5 Frequency Response of RWM Alone

A detailed account of the RWM circuitry can be found in the paper, "An Improved Resistive Wall Current Monitor," by Jim Crisp and Brian Fellenz [2]. In this paper the actual response of the wall current monitor was found using a test setup that allowed a current to be passed through the center of the RWM. Figure 11 shows the response through the RWM to be flat up to 4 GHz while the response through the calibration port starts rolling off at 2 GHz. This suggests that the dispersion caused by the RWM cables leading to the calibration port and from the RWM are the primary source of signal variations.

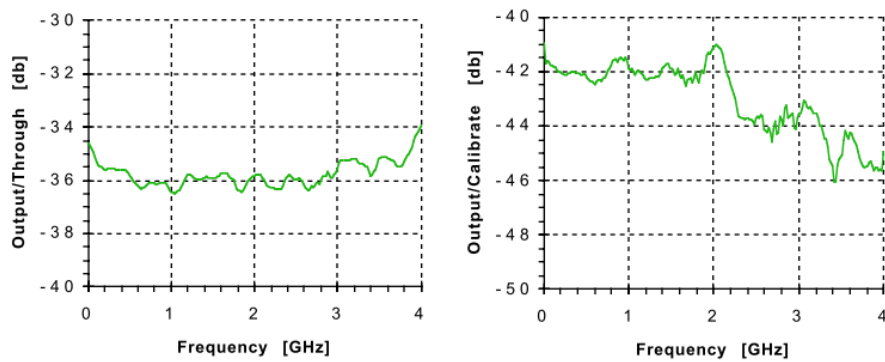


Figure 11: The left image shows the frequency response of the RWM found by Brian Fellenz and Jim Crisp using a current through the center of a Main Injector style RWM on a test stand. The right image shows the response through the calibration port on this RWM. This data shows that the RWM itself has a flat frequency response up to 4 GHz while the calibration port response rolls off after 2 GHz [2].

6 Time Domain Cable Analysis

Section 5 suggests that a thorough understanding of the cables used for the RWM is essential to understanding their effect on the beam signal. The cable that leads from the service building to the calibration port of the RWM is Andrew LDF4-50A 1/2 Inch Heliax. The readback from the RWM to the service building is through Andrew LDF5-50A 7/8 Inch Heliax. Since the cable is in position with one end in the MI12 service building and the other in the tunnel, an S21 measurement for frequency response is quite tricky. Instead we performed time domain analysis by once again passing a short pulse through the cables and measuring the signal at the other end with an oscilloscope. Due to availability, a different signal generator and oscilloscope were used for this portion of the test. A 6 ns -5 V pulse was passed through both cables and collected at a 5 GHz rate. The results of this test are displayed in figure 12. Both cables influence the short pulse in a similar fashion though the 7/8 Inch cable certainly performs slightly better.

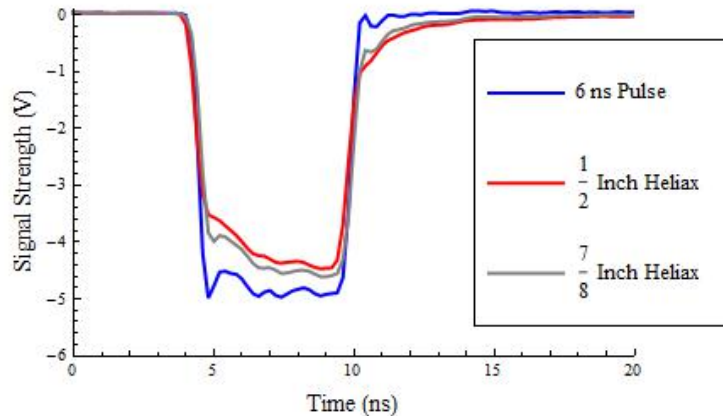


Figure 12: By measuring a 6 ns pulse and then measuring the same pulse through both the calibration port cable and the readback cable, the cable effects can be better understood.

Using the the deconvolution of the output signal with the input signal as described in section 2, the impulse response for the cable is found. Since only the larger 7/8 Inch heliax will influence the output signal, it is the only one analyzed here. This impulse response is in the time domain with 2×10^{-10} Seconds between each sample point as were the signals from which it was derived. The impulse response, shown in figure 13, is limited by the frequency content of the pulse supplied for its measuring.

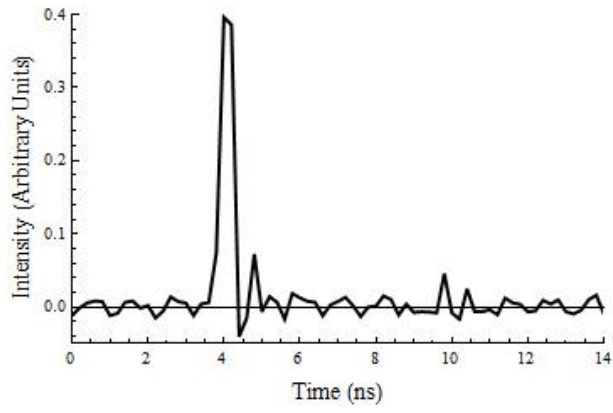


Figure 13: The impulse response is found by deconvolving the original signal from that measured at the other end of the 7/8 Inch heliax.

7 Theoretical Cable Analysis

The theoretical response of a coaxial cable to a step function is described by equation 4 where bl is 1.45×10^{-8} times the total cable attenuation at 1 GHz and erf is the error function as described in equation 5 [7] [8].

$$V_{out} = V_{in}(1 - erf[\frac{bl}{\sqrt{2t}}]) \quad (4)$$

$$erf(x) = \int_0^x e^{-t^2} dt \quad (5)$$

The attenuation at 1 GHz from the Andrews data sheet for 7/8 Inch heliax is .412 dB per meter. Using a pulse generator and an oscilloscope, the cable was found to be 198 ns long. The Andrews cable has a phase velocity of 89% the speed of light. From this measurement the cable length was found to be approximately 53 m. The total attenuation from the cable is therefore 2.178 dB.

The impulse response of the cable can be found by taking the derivative of equation 4. With a continuous function describing the impulse response, one can create a table based on any chosen sampling rate. Figure 14 shows a table of points with 2×10^{-10} Sec between each point which is the sampling rate used in section 6. Figure 15 shows the original signal from section 6 convolved with the impulse response found theoretically from equation 4.

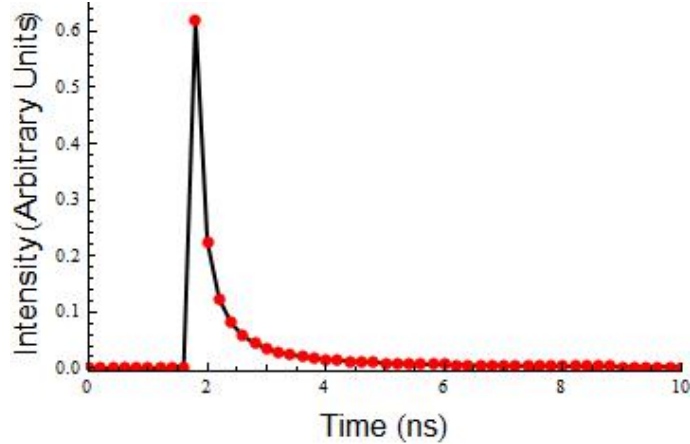


Figure 14: This is the theoretical impulse response of the $\frac{7}{8}$ in HeliAx used to monitor the MiniBooNE RWM.

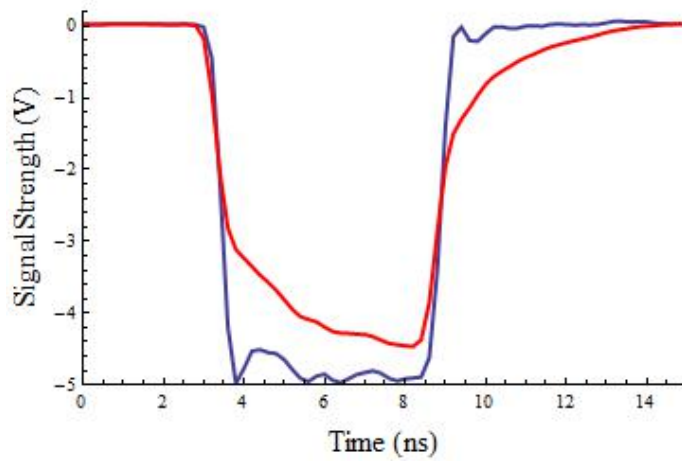


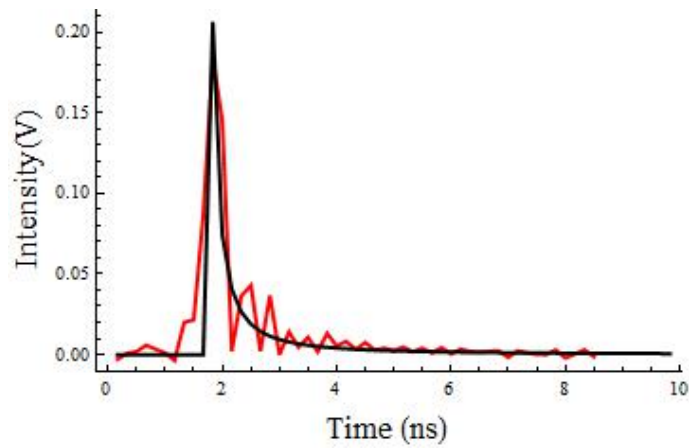
Figure 15: The theoretical signal output is displayed here in red with the original signal in blue. The red trace is found by convolving the original signal from section 6 with the theoretical impulse response from figure 14. The shaping of the theoretical impulse response is consistent with that of observations from section 6.

8 Error Analysis

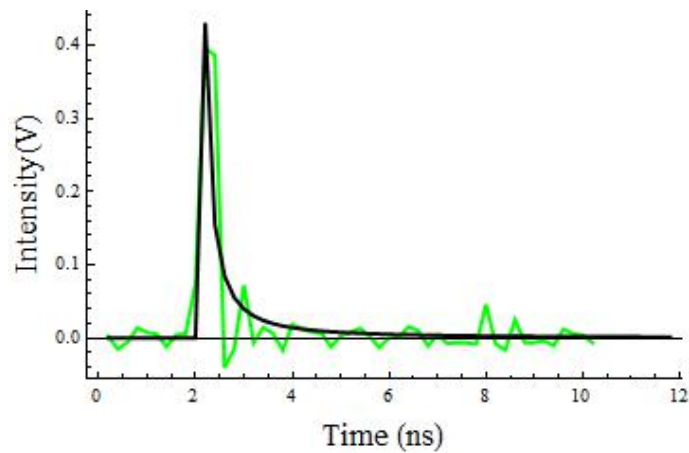
The theoretical impulse response from section 7 can now be compared to the impulse responses that were measured in sections 4 and 6. In section 4, the impulse response was found by performing a network analyzer measurement to find the frequency response of the system from through the $\frac{1}{2}$ in calibration port cable, into the RWM and then out of the RWM through the $\frac{7}{8}$ in cable. This was then converted into an impulse response through the inverse Fourier transform. Figure 16(a) shows the theoretical impulse response plotted with this measured impulse response. In section 6 a square pulse was measured before the $\frac{7}{8}$ in cable and after propogating through the cable. Deconvolution is then used to find the measured impulse response. The theoretical impulse response compared to this measured impulse response is shown in figure 16(b).

The standard error of these fits is calculated using equation 6 where n represents the sample number, $f(n)$ represents the theoretical function value at that sample number, and $m(n)$ represents the measured value at that sample number [9]. A multiplier is required to match the theoretical impulse response to the measured. This multiplier was determined for each case by varying the multiplier to minimize the standard error. The standard error for the case using the calibration port was 1.9% while the standard error for the case using just the $\frac{7}{8}$ in cable was 4.3%. Thus, the function determined using equation 4 is a viable representation within 5% of measured values for the impulse response.

$$StandardError = \sqrt{\frac{\sum [f(n) - m(n)]^2}{n - 2}} \quad (6)$$



(a) The standard error of the impulse response found using a network analyzer through the RWM calibration port and cables compared to the theoretical impulse response is 1.9%



(b) The standard error of the impulse response found using a square pulse through the $\frac{7}{8}$ inch readback cable was found to be 4.3%.

Figure 16: There is a less than 5% error between measurements and theoretical values.

9 Conclusion

In conclusion the pulse shaping demonstrated through time domain measurements of an 8 ns pulse causes asymmetries consistent with asymmetries seen in RWM data. These measurements suggest that the asymmetries as illustrated in figure 2 are not representative of longitudinal asymmetries in the energy distribution of the beam. The theoretical impulse response explained in section 7 agrees with measured data to within 5% thus making it a viable function for representation of the response of the RWM. The impulse responses found in this paper can be used to deconvolve a better description of the beams actual longitudinal distribution.

10 Acknowledgements

Thanks to Tom Kobilarcik, Richard Van De Water, Michael Wren, Cindy Joe, Adam Watts and Dennis Barak for their assistance with this research.

References

- [1] R. C. Webber, “Tutorial on Beam Current Monitoring”, Fermilab-Conf-00-119, Fermilab, June 2000.
- [2] B. Fellenz and J. Crisp, “An Improved Resistive Wall Monitor”, Beam Instrumentation Workshop, SLAC, Stanford CA, AIP Conference Proceedings 451, 1998 pp. 502-506.
- [3] B. Fellenz and J. Crisp, “Calibration of the Resistive Wall Monitor for the SBD and FBI Systems”, Fermilab TM-2208, June 1,2003.
- [4] P. Odier, “A New Wide Band Wall Current Monitor”, DIPAC’2003, Mainz, Germany, 2003.
- [5] Steven W. Smith *The Scientist and Engineer’s Guide to Digital Signal Processing*. California Technical Publishing, San Diego, California, 1997 pg. 177.
- [6] Real-Time Versus Equivalent-Time Sampling 2001. Retrieved January 2, 2013, from www.tek.com/document/application-note/real-time-versus-equivalent-time-sampling.
- [7] R. Thurman-Keup, C. Bhat, W. Blokland, J. Crisp, N. Eddy, B. Fellenz, R. Flora and A. Hahn *et al.*, “Longitudinal bunch monitoring at the Fermilab Tevatron and Main Injector synchrotrons,” JINST **6**, T10004 (2011) [arXiv:1110.3086 [physics.ins-det]].
- [8] Q. Kerns et al., “Pulse response of coaxial cables”, in LRL counting handbook , Lawrence Radiation Laboratory, University of California, Berkeley, California, U.S.A., (1996).

- [9] J. McClave; F. Dietrich; T. Sincich, "Statistics, Seventh Edition", Prentice Hall, Upper Saddle River, New Jersey, (1997).